

01 Aug 2008

# Reconstruction of Dispersive Dielectric Properties for PCB Substrates using a Genetic Algorithm

Jianmin Zhang

Marina Koledintseva
*Missouri University of Science and Technology*, marinak@mst.edu

James L. Drewniak
*Missouri University of Science and Technology*, drewniak@mst.edu

David Pommerenke
*Missouri University of Science and Technology*, davidjp@mst.edu

*et. al. For a complete list of authors, see https://scholarsmine.mst.edu/ele_comeng_facwork/1238*



## Recommended Citation

J. Zhang and M. Koledintseva and J. L. Drewniak and D. Pommerenke and R. E. DuBroff and Z. Yang and W. Cheng and K. Rozanov and A. Orlandi and G. Antonini, "Reconstruction of Dispersive Dielectric Properties for PCB Substrates using a Genetic Algorithm," *IEEE Transactions on Electromagnetic Compatibility*, vol. 50, no. 3, pp. 704-714, Institute of Electrical and Electronics Engineers (IEEE), Aug 2008. The definitive version is available at https://doi.org/10.1109/TEMC.2008.927923

# Reconstruction of Dispersive Dielectric Properties for PCB Substrates Using a Genetic Algorithm

Jianmin Zhang, *Member, IEEE*, Marina Y. Koledintseva, *Senior Member, IEEE*, James L. Drewniak, *Fellow, IEEE*, David J. Pommerenke, *Senior Member, IEEE*, Richard E. DuBroff, *Senior Member, IEEE*, Zhiping Yang, *Senior Member, IEEE*, Wheling Cheng, Konstantin N. Rozanov, Giulio Antonini, *Senior Member, IEEE*, and Antonio Orlandi, *Fellow, IEEE*

***Abstract*—An effective method for extracting parameters of a Debye or a Lorentzian dispersive medium over a wideband frequency range using a genetic algorithm (GA) and a transmission-line model is presented. Scattering parameters ($S$-parameters) of the transmission-line sections, including a parallel plate, microstrip, and stripline, are measured. Wave equations for TEM/quasi-TEM mode with a complex propagation constant and a frequency-dependent wave impedance are used to evaluate the corresponding $S$-parameters in an analytical model. The discrepancy between the modeled and measured $S$-parameters is defined as the objective function in the GA. The GA is used for search of the dispersive-medium parameters by means of minimizing the objective function over the entire frequency range of interest. The reconstructed Debye or Lorentzian dispersive material parameters are corroborated by comparing the original measurements with the FDTD modeling results. The self-consistency of the proposed method is demonstrated by constructing different test structures with an identical material, i.e., material parameters of a substrate extracted from different transmission-line configurations. The port effects on the material parameter extraction are examined by using through-reflection-line calibration.**

***Index Terms*—Electromagnetic propagation in dispersive media, finite-difference time-domain (FDTD) methods, genetic algorithms (GAs), scattering parameters, transmission lines.**

## I. Introduction

THE KNOWLEDGE of complex dielectric properties of materials is fundamental in the study of electromagnetic energy absorption, high-speed integrated circuit package design, and high-speed signal link path characterization [1]–[4]. Numerous methods are available for determining different ranges of the values of permittivity and permeability [1]–[8]. Each technique has its advantages and disadvantages. The resonant-cavity methods are comparatively accurate and applicable at higher frequencies (microwaves), but the measurements are narrowband. Coaxial-line techniques achieve wideband material property extraction with no leakage and radiation losses, but are most amenable to powders or liquids, and the port de-embedding is difficult. Dielectric constant and loss tangent can be measured using an impedance analyzer, but the application is limited at low frequency. The above-mentioned techniques extract material properties over a certain frequency range that is usually not sufficient for wideband digital pulses. A short-pulse propagation technique can be used to obtain dielectric properties for printed circuit board (PCB) substrate materials based on a circular capacitor and a stripline structure in the time domain up to 30 GHz [9]. This technique is limited in its practical manufacturing capabilities, bandwidth of the test setup, and an inherent signal-to-noise ratio of the time-domain measurement [9]. Herein, the different technique associated with scattering parameters ($S$-parameters) measurements for obtaining material properties is presented. It is based on approximating the frequency dependences by the Debye or Lorentzian dispersion laws, and a genetic algorithm (GA). Using this technique, the dispersive material properties can be presented in a continuous functional form. They are easy to implement in full-wave modeling, and can be used over a wide frequency span [10]–[12].

To simulate the wideband electromagnetic response of complex structures, it is necessary to know the frequency dispersion laws of the bulk material constituting the structures. Traditionally, the Debye and Lorentzian laws are used as the simplest ones of frequency dispersion [12]–[14]. More general, the dispersion laws may be approximated by a sum of several Debye and/or Lorentzian terms. Using the general dispersion law, it is possible to fit physically realizable dielectric behavior, i.e., obeying the Kramers–Kronig causality relations and fitting the frequency dependence of permittivity [13].

Development of a simple, accurate, and reliable method to extract Debye or Lorentzian dispersive medium parameters from measured $S$-parameters is beneficial, as $S$-parameters characterize transmission lines in a wide frequency span precisely. However, characterizing the Debye or Lorentzian medium from a set of measured data typically requires the solution of systems of nonlinear equations, as indicated in [15], which is cumbersome. In addition, the number of frequency points of the measured $S$-parameters is much greater than the number of unknowns to be extracted for dispersive materials. Moreover, measured $|S_{11}|$ curve and phase $S_{21}$ curve are usually with multipeak, which is a typical multimodal optimization problem. This motivates the application of GAs with the characteristic of powerful, robust, and effective in global searching and optimization especially for solving multimodal problems [16]–[19].

Manuscript received January 5, 2007; revised January 10, 2008.

J. Zhang and W. Cheng are with Cisco Systems, Inc., San Jose, CA 95134 USA (e-mail: jianmin@cisco.com; wheling@cisco.com).

M. Y. Koledintseva, J. L. Drewniak, D. J. Pommerenke, and R. E. DuBroff are with Missouri University of Science and Technology (formerly University of Missouri-Rolla), Rolla, MO 65409 USA (e-mail: marinak@mst.edu; drewniak@mst.edu; davidjp@mst.edu; red@mst.edu).

Z. Yang is with Nuova Systems, Inc., San Jose, CA 95134 USA (e-mail: zyang@nuovasystems.com).

K. N. Rozanov is with the Institute for Theoretical and Applied Electromagnetics, Russian Academy of Sciences, Moscow 125412, Russia (e-mail: k_rozanov@mail.ru).

G. Antonini and A. Orlandi are with the University of L'Aquila, L'Aquila I-67010, Italy (e-mail: antonini@ing.univaq.it; orlandi@ing.univaq.it).

Color versions of one or more of the figures in this paper are available online at http://ieeexplore.ieee.org.

Digital Object Identifier 10.1109/TEMC.2008.927923

In this paper, Section II gives the description of the dispersion laws used in the material parameter extraction. Implementation of GAs to extract material parameters is discussed in this section as well. Analytical formulations for the calculation of $S$-parameters based on the per-unit-length (p.u.l.) resistance, inductance, conductance, and capacitance (*RLGC*) parameters and wave impedance $Z_w$ for planar transmission lines are contained in Section III. Case studies are shown in Section IV where a layer of composite carbon- and aluminum-filled dielectric and fiberglass epoxy FR4 substrates are investigated. The extracted dispersive parameters are verified by comparing the measured and the full-wave FDTD modeled $S$-parameters for different cases. Port effects, self-consistency, and sensitivity analysis are also discussed in this section. The conclusion is summarized in Section V.

## II. Application of a Genetic Algorithm and Dispersion Laws of Debye and Lorentzian

The permittivity of a nonmagnetic, linear, isotropic, and homogeneous dispersive material can be described in a general form

$$\varepsilon(\omega) = \varepsilon_0\varepsilon_\infty + \varepsilon_0 \sum_{k=1}^{M} \frac{A_k\omega_{0k}^2}{\omega_{0k}^2 - \omega^2 + j\omega(2\delta_k)} + \varepsilon_0 \sum_{i=1}^{N} \frac{A_i}{1 + j\omega\tau_i} - \frac{j\sigma_e}{\omega} \quad (1)$$

where $A_k$ or $A_i$ is a Lorentzian or a Debye dielectric susceptibility amplitude, which is the difference between the static dielectric constant $\varepsilon_{sk}$ (or $\varepsilon_{si}$) and the high-frequency ("optical") relative permittivity $\varepsilon_\infty$. $\omega_{0k}$ and $(2\delta_k)$ are the resonant frequency and the width of the $k$th Lorentzian peak. The relaxation time constant $\tau_i$ is for the $i$th Debye component. The free-space permittivity is $\varepsilon_0$, and $\sigma_e$ is the effective conductivity. If (1) is simplified to a one-term Debye, it can be rewritten as

$$\varepsilon(\omega) = \varepsilon_0\varepsilon_\infty + \varepsilon_0 \frac{\varepsilon_s - \varepsilon_\infty}{1 + j\omega\tau} - \frac{j\sigma_e}{\omega}. \quad (2)$$

The real part and the imaginary part of the relative permittivity $(\varepsilon_r = \varepsilon_r' - j\varepsilon_r'')$ are

$$\begin{cases} \varepsilon_r'(\omega) = \dfrac{\varepsilon_s + \varepsilon_\infty(\omega\tau)^2}{1 + (\omega\tau)^2} \\ \varepsilon_r''(\omega) = \dfrac{(\varepsilon_s - \varepsilon_\infty)\omega\tau}{1 + (\omega\tau)^2} + \dfrac{\sigma_e}{\omega\varepsilon_0}. \end{cases} \quad (3)$$

Similarly, for a single-component Lorentzian dielectric material, (1) is simplified to

$$\varepsilon(\omega) = \varepsilon_0\varepsilon_\infty + \varepsilon_0 \frac{(\varepsilon_s - \varepsilon_\infty)\omega_0^2}{\omega_0^2 - \omega^2 + j\omega(2\delta)} - \frac{j\sigma_e}{\omega} \quad (4)$$

and the real part and the imaginary part of the relative permittivity for the Lorentzian material are

$$\begin{cases} \varepsilon_r'(\omega) = \dfrac{(\omega_0^2 - \omega^2)(\varepsilon_s\omega_0^2 - \varepsilon_\infty\omega^2) + 4\varepsilon_\infty(\omega\delta)^2}{(\omega_0^2 - \omega^2)^2 + 4(\omega\delta)^2} \\ \varepsilon_r''(\omega) = \dfrac{2\omega\delta\omega_0^2(\varepsilon_s - \varepsilon_\infty)}{(\omega_0^2 - \omega^2)^2 + 4(\omega\delta)^2} + \dfrac{\sigma_e}{\omega\varepsilon_0}. \end{cases} \quad (5)$$

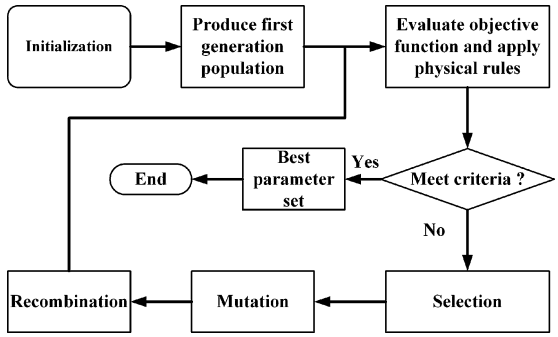


Fig. 1. GA program flowchart.

GAs are optimization techniques based on the mechanics of natural selection and natural genetics [16]–[19]. The heuristic nature of GAs makes them effective for solving complex, multimodal, and high-dimensional problems. GAs operate on a population of solutions, while the traditional optimization techniques (hill climbing, enumerative, and random search) work on a single solution. The widely used hill-climbing search technique is based on the assumption that the problem domain being worked at is continuous, and/or at least the first-order derivatives of the functions used to represent the problem in the domain exist. However, the constraints (differentiability or continuity) are difficult, or even impossible to deal with in some practical problems, especially at boundaries or interfaces with discontinuities. Since this kind of search technique is highly dependent on the local gradient and starting search point, the convergence rate may be faster than that of GAs, but getting "stuck" in a local optimum is their major drawback if the problem space is multimodal. In contrast with the hill-climbing search techniques, optima from a GA are based on the entire population, and the GA is a global search technique. As for enumerative techniques and random search techniques, they are inefficient in solving optimization problems because of their search mechanisms based on random searching only, or point-to-point mapping. However, GAs are a kind of random search, but they are associated with the directions and chances in the problem domain from the previously searched results, and they are, therefore, efficient. Furthermore, physical rules can be implemented in GAs, which makes them more flexible and effective in solving practical optimization problems.

To implement a GA for solving an optimization problem, it is necessary to formulate the problem mathematically by defining an objective function, building up an analytical model, and choosing GA operators, such as selection, recombination, and mutation [16]. To build up analytical models for different transmission-line structures is detailed in Section III. The GA program flowchart is shown in Fig. 1. An example of the GA convergence curve and a parameter extraction convergence curve is shown in Fig. 2. Two different objective functions are defined for different calibration methods used in $S$-parameter measurements. For one of the stripline measurements, through-reflect-line (TRL) calibration is used to remove SMA port effects, while short-open-load-through (SOLT) calibration is used for the other cases. The objective function for the measurement with TRL calibration is defined based on the differences of both the magnitude and the phase of $S_{21}$ between the measurement and the analytical modeling as the reflection $(S_{11})$ with a

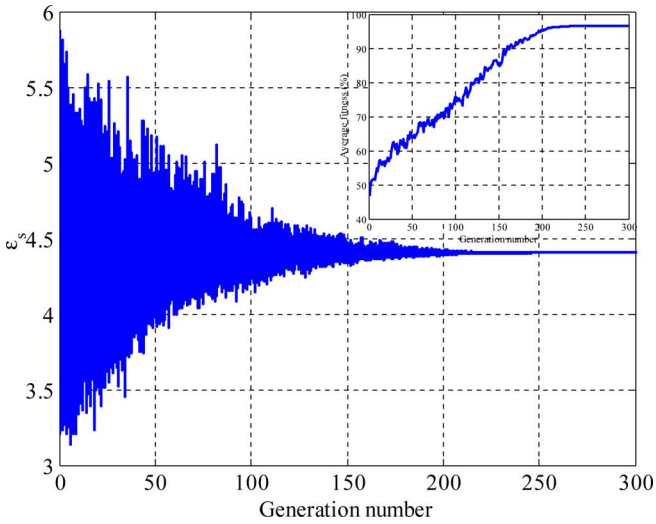


Fig. 2. Example of the GA convergence curve and the parameter extraction convergence curve.

TRL calibration is very weak from the measurement. For SOLT calibration, the magnitude differences of both $S_{11}$ and $S_{21}$ contribute to the objective function. Two defined objective functions are summarized (6), as shown at the bottom of the page.

The magnitudes of $S$-parameters at frequency $f_i$, $|S_{11}^m(f_i)|$ and $|S_{21}^m(f_i)|$, are obtained from measurement, while $|S_{11}^e(f_i)|$ and $|S_{21}^e(f_i)|$ are evaluated from analytical modeling (6). $P_{21}^m(f_i)$ and $P_{21}^e(f_i)$ are the $S_{21}$ phase from measurement and analytical modeling, respectively. The terms $\max|S_{11}^m|$, $\max|S_{21}^m|$, and $\max|P_{21}^m|$ are the maximum absolute value of $|S_{11}|$, $|S_{21}|$, and $S_{21}$ phases from measurement. The purpose of introducing the maximum terms in (6) is to normalize each difference term to make each one equally weighted and the objective function $\Delta$ unitless. The expected parameters of the dispersive medium are found as the objective function is minimized.

## III. Analytical Models for Different Planar Transmission Lines and Their Application Limitations

Analytical models for parallel-plate, microstrip, and strip transmission lines with dispersive dielectric substrates are studied and a general form of two-port $S$-parameters is formulated in this section. Limitations of the proposed method for each transmission-line structure are discussed as well. Assuming that higher order modes and radiation because of the fringing fields and surface waves are negligible for a transmission line, and considering that only the TEM (quasi-TEM for microstrip) wave is excited by a 1-V voltage source with an angular frequency $\omega$, the

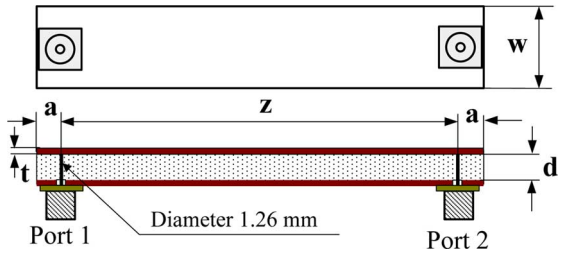


Fig. 3. Parallel-plate transmission-line structure.

$S$-parameters for the transmission line can be calculated with the propagation constant $\gamma$ and the wave impedance $Z_W$ as [20]

$$|S_{11}| = 20\log_{10}\left|\frac{Z_{\text{in}} - R_0}{Z_{\text{in}} + R_0}\right| \tag{7}$$

$$|S_{21}| = 20\log_{10}\left|\frac{2Z_{\text{in}}(1+\Gamma_l)}{(Z_{\text{in}} + R_0)(e^{-\gamma z} + \Gamma_l e^{\gamma z})}\right| \tag{8}$$

$$P_{21} = \text{angle}\left(\frac{2Z_{\text{in}}(1+\Gamma_l)}{(Z_{\text{in}} + R_0)(e^{-\gamma z} + \Gamma_l e^{\gamma z})}\right) \tag{9}$$

where $z$ is the transmission-line length, and the input impedance can be evaluated from

$$Z_{\text{in}} = \frac{V(-z)}{I(-z)} = Z_W\frac{R_0 + Z_W\tanh(\gamma z)}{Z_W + R_0\tanh(\gamma z)} \tag{10}$$

$R_0$ is the load resistance, which is assumed to be equal to the resistance at the excitation port. The reflection coefficient at the load is determined from

$$\Gamma_l = \frac{R_0 - Z_W}{R_0 + Z_W} \tag{11}$$

where the origin of the transmission line is defined at the load. If an extra length of an open stub exists at a port (often the case for vertical SMA launch ports in a parallel-plate configuration), then the open stub effects are necessary to be considered both in the input impedance and load impedance with a suitable model. Since the propagation constant $\gamma$ and the wave impedance $Z_W$ can be evaluated from a set of *RLGC* parameters, to represent the *RLGC* parameters through the substrate dielectric properties, i.e., $\varepsilon_r'$ and $\varepsilon_r''$, the dimensions of the transmission line are needed.

### A. Parallel-Plate Transmission Lines

The simplest transmission-line structure for experimental implementation is a parallel-plate transmission line shown in Fig. 3. The known expressions [21] for p.u.l. *RLGC* parameters with frequency-dependent permittivity of a substrate can be

$$\begin{cases} \Delta = \dfrac{1}{N}\sqrt{\displaystyle\sum_{i=1}^{N}\left\{\left[\frac{|P_{21}^m(f_i) - P_{21}^e(f_i)|}{\max|P_{21}^m|}\right]^2 + \left[\frac{||S_{21}^m(f_i)| - |S_{21}^e(f_i)||}{\max|S_{21}^m|}\right]^2\right\}}, & \text{for TRL calibration} \\ \Delta = \dfrac{1}{N}\sqrt{\displaystyle\sum_{i=1}^{N}\left\{\left[\frac{||S_{11}^m(f_i)| - |S_{11}^e(f_i)||}{\max|S_{11}^m|}\right]^2 + \left[\frac{||S_{21}^m(f_i)| - |S_{21}^e(f_i)||}{\max|S_{21}^m|}\right]^2\right\}}, & \text{for SOLT calibration} \end{cases} \tag{6}$$

used directly as

$$R = \frac{2R_s}{w} + R_{\rm dc} \tag{12}$$

$$L = \frac{\mu d}{w} \tag{13}$$

$$G = \frac{\omega\varepsilon''(\omega)w}{d} = \frac{\omega w\varepsilon_r''(\omega)\varepsilon_0}{d} \tag{14}$$

$$C = \frac{\varepsilon'(\omega)w}{d} = \frac{\varepsilon_r'(\omega)\varepsilon_0 w}{d} \tag{15}$$

where $w$ is the strip width and $d$ is the separation of two metal plates. The surface resistance is

$$R_s = \sqrt{\frac{\omega\mu_0}{2\sigma}}. \tag{16}$$

The d.c. resistance is calculated as

$$R_{\rm dc} = \frac{2}{tw\sigma} \tag{17}$$

where $t$ is the thickness of the conductor and $\sigma$ is the conductivity (assuming that two metal plates are identical). The TEM wave propagation constant and characteristic impedance are

$$\gamma = \sqrt{\omega\left(\frac{2R_s}{d} + j\omega\mu\right)(\varepsilon'' + j\varepsilon')} \tag{18}$$

$$Z_W = \frac{d}{w}\sqrt{\frac{(2R_s/\omega d) + j\omega\mu}{\varepsilon'' + j\varepsilon'}}. \tag{19}$$

To study the frequency behavior for various substrates over different frequency spans using a parallel-plate structure, it is necessary to design the structure with different dimensions. The TEM assumption is true for a parallel-plate structure only over a certain frequency range, depending on its configuration. To hold the TEM assumption, referring to Fig. 3, the ratio of the transmission-line width to its thickness must meet $w/d >> 1$, which should be at least 10–20. It is assumed here that an acceptable ratio is $w/d \geq 15$. The critical wavelength of the first higher order mode based on a perfect electrical conductor (PEC) boundary condition is defined as [21]

$$\lambda_{c1} = 2d. \tag{20}$$

Since the fringing fields in the parallel-plate structure are neglected, it is reasonable to apply perfect magnetic conductor (PMC) boundary conditions at the two sidewalls along the direction of wave propagation to see a longer cutoff wavelength with $w > d$ [22]

$$\lambda_{c1}' = 2w. \tag{21}$$

The first cutoff frequency is then determined from $\max(\lambda_{c1}, \lambda_{c1}')$ as

$$f_{c1} = \frac{c_0}{2w\sqrt{\varepsilon_r}}. \tag{22}$$

The highest frequency $f_1$ (in hertz) and the thickness of the dispersive layer medium $d$ (in millimeters) for only TEM wave propagation satisfy the condition

$$d \cdot f_1 < \frac{100c_0}{3\sqrt{\varepsilon_r}} \tag{23}$$

where $c_0$ (in meters per second) is the speed of light in free space and $\varepsilon_r$ is the estimated relative permittivity of the medium, or for the dispersive medium, the maximum real part of the permittivity in the frequency range of interest.

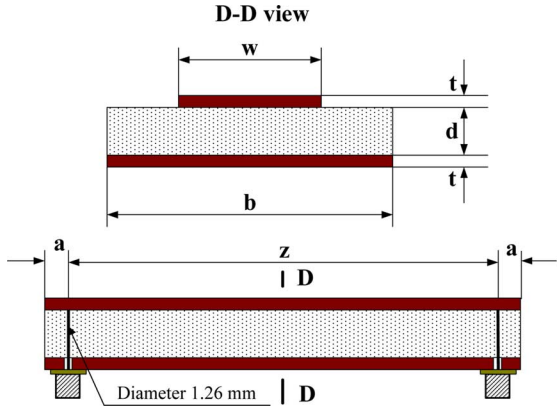


Fig. 4. Geometry of a microstrip transmission line.

### *B. Microstrip Transmission Lines*

Poh *et al.* derived analytical and semiempirical formulas for the calculation of microstrip-line capacitance and line impedance [23]. If the relative permittivity of the substrate of the microstrip line is in the range of $1 < \varepsilon_r < 16$, and the ratio of the substrate thickness to the microstrip trace width is limited to the range of $0.1 \leq (d/w) \leq 0.5$, the p.u.l. capacitance can be calculated using

$$C = \frac{w\varepsilon_r'\varepsilon_0}{d}\left\{1 + \frac{2d}{\pi\varepsilon_r' w}\left[\ln\left(\frac{w}{2d}\right) + 1.416\varepsilon_r' + 1.547 + (1.112 - 0.028\varepsilon_r')\frac{d}{w}\right]\right\} \tag{24}$$

where $d$ is the dielectric thickness and $w$ is the width of the microstrip trace, as shown in Fig. 4. The quasi-TEM wave impedance can be approximated by (25), as shown at the bottom of the page.

Similar to the discussion in Section III-A, the p.u.l. resistance can be obtained from

$$R = \left(\frac{1}{w} + \frac{1}{b}\right)\left(R_S + \frac{1}{\sigma t}\right) \tag{26}$$

where $t$ is the thickness of the conductor and $b$ is the width of the reference. The p.u.l. shunt conductance $G$ can be found from

$$G = \omega C\frac{\varepsilon_r''}{\varepsilon_r'}. \tag{27}$$

$$Z_w = \frac{377d}{w\sqrt{\{\varepsilon_r' - (2d/\pi w)\left[(1+\varepsilon_r')\ln(2d/w) - 2.23 - 4.554\varepsilon_r' - (4.464 + 3.89\varepsilon_r')\,d/w\right]\}}} \tag{25}$$

The p.u.l. inductance of the microstrip line can be evaluated from

$$L = \frac{1}{\omega}\sqrt{\left[G^2 + (\omega C)^2\right]|Z_W|^4 - R^2}. \tag{28}$$

The complex wave propagation constant $\gamma$ and wave impedance $Z_w$ are calculated as the p.u.l. parameters are known. If $\varepsilon_r'$ of the substrate is larger than 16, or the ratio of the substrate thickness to the trace width is out of the range of 0.1–0.5, expressions for the p.u.l. capacitance and the TEM wave impedance calculation can be found in [23] as well.

Three mechanisms may limit the application of microstrip configurations: higher order modes, surface-wave propagation in the planar metal–dielectric–air structure, and radiation effects with the open structure. The upper bound frequency can be estimated based on the three mechanisms and determined from the lowest one. The cutoff frequency for the first higher order mode is estimated as [24]

$$f_c = \frac{c_0}{\sqrt{\varepsilon_r'}(2w + 0.8d)} \tag{29}$$

where $c_0$ is the speed of light in free space. The lowest TM surface-wave mode has no cutoff frequency, but its coupling to the quasi-TEM mode becomes significant only when their phase velocities are nearly matched. This occurs at frequency [24]

$$f_s = \frac{c_0 \arctan(\varepsilon_r')}{\sqrt{2}\pi d\sqrt{\varepsilon_r' - 1}}. \tag{30}$$

An approximate relation for the frequency where the radiation becomes significant is [24]

$$f_r d > 2.14\sqrt[4]{\varepsilon_r'} \tag{31}$$

where $f_r$ is in gigahertz and $d$ is in millimeters.

### C. Stripline

For a symmetric stripline structure shown in Fig. 5, if the ratio of the trace width to the spacing between the two reference planes is greater than 0.35, i.e., $w/(2d) > 0.35$, a wide stripline is defined [25]. The calculation of the p.u.l. parameters *RLGC* for a wide stripline can be performed by using [26]. The p.u.l. resistance is calculated as

$$R = \frac{1}{2}\left(R_S + \frac{1}{\sigma t}\right)\left(\frac{1}{w} + \frac{1}{b}\right). \tag{32}$$

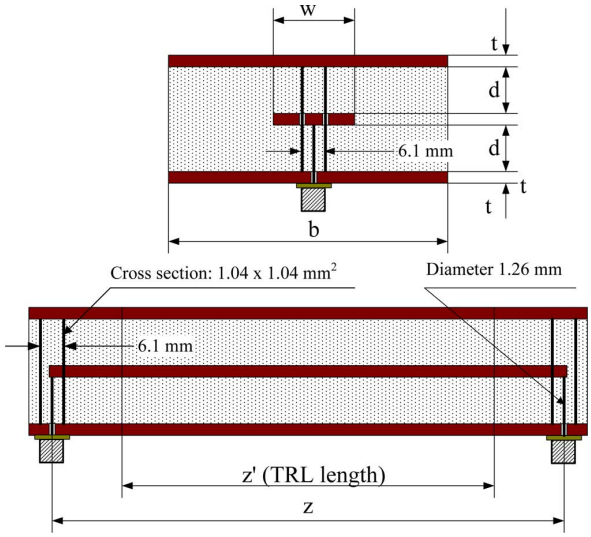


Fig. 5. Geometry of a strip transmission line.

Equation (33), shown at the bottom of the page, gives the p.u.l. inductance, and the p.u.l. capacitance is

$$C = 3.5427 \times 10^{-11}\varepsilon_r'\left\{\frac{w}{2d} + \frac{1}{\pi}\left\{\frac{2d+t}{d}\ln\left[\frac{4d+t}{2d}\right] - \frac{t}{2d}\ln\left[\frac{t(4d+t)}{4d^2}\right]\right\}\right\}. \tag{34}$$

The TEM wave impedance is evaluated from (35), shown at the bottom of the page.

The p.u.l. shunt conductance $G$ can be found from

$$G = \sqrt{\frac{\left[R^2 + (\omega L)^2\right]}{|Z_W|^4} - (\omega C)^2}. \tag{36}$$

The complex wave impedance is recalculated using the known p.u.l. parameters, and is then used in the GA model for estimating $S$-parameters. For a wide stripline, the cutoff frequency of the first higher order mode is estimated as [27]

$$f_{c1} = \frac{15}{\sqrt{\varepsilon_r'}\,(w + (2d+t)\,\pi/4)} \tag{37}$$

where $w, d$, and $t$ are in centimeters, and $f_{c1}$ is in gigahertz, referring to Fig. 5. Surface waves and fringing fields can be neglected since the containment of the field in a stripline structure is much better than in a microstrip or a parallel-plate structure.

$$L = \frac{3.14 \times 10^{-7}}{(w/2d) + (1/\pi)\left\{(2d + t/d)\ln\left[4d + t/2d\right] - (t/2d)\ln\left[t\,(4d+t)\,/4d^2\right]\right\}} \tag{33}$$

$$Z_w = \frac{94.15}{(w/2d) + (1/\pi)\left\{(2d + t/d)\ln\left[4d + t/2d\right] - (t/2d)\ln\left[t\,(4d+t)\,/4d^2\right]\right\}}\frac{1}{\sqrt{\varepsilon_r}} \tag{35}$$

TABLE I
DIMENSIONS OF FOUR PARALLEL-PLATE TRANSMISSION LINES AND THEIR MAXIMUM MEASUREMENT FREQUENCIES

| Board | $f_{measured\text{-}max}$ (GHz) | w (mm) | d (mm) | z (mm) | a (mm) | t (mm) |
|---|---|---|---|---|---|---|
| #1 | 5 | 15 | 0.39 | 79.1 | 4.3 | 0.04 |
| #2 | 4.5 | 15.2 | 1.06 | 51.6 | 4 | 0.07 |
| #3 | 3.3 | 20 | 1.55 | 59.2 | 4.1 | 0.05 |
| #4 | 10 | 10 | 0.6 | 50 | 5 | 1.5 |

## IV. CASE STUDIES AND SENSITIVITY ANALYSIS

Six cases, including one microstrip, one stripline, and four parallel plates (1–4), are studied based on the proposed method. The substrate used in the parallel-plate test board 4 is a strong dispersive composite material. FR4, a weak dispersive substrate, is used in the other five cases, which is a glass-filled epoxy resin material, and is widely used in the PCBs and easy to find for study. It is known that the relative permittivity of FR4 varies substantially with frequency and differs for different samples of the material. To check the self-consistency of the proposed method, a same sample material is applied to construct the parallel-plate test board 1 and the microstrip test board. Different dimensions of parallel-plate test boards demonstrate the application limitation given in (23) for parallel-plate transmission-line configurations. The sensitivity analysis is discussed in the parameter extraction for the parallel-plate test board 1.

### A. Parallel-Plate Cases

Three parallel-plate test boards (1–3) were made from different double-sided copper-clad boards with FR4 substrates. The test board 4 was constructed by filling a composite dielectric sheet between two copper plates. The bottom and front views of the parallel-plate structure are schematically shown in Fig. 3. Debye dielectric parameter extractions were applied on FR4 materials for boards 1, 2, and 3, while Lorentzian parameter extraction was implemented in the board 4. $S$-parameters were measured using an HP 8720ES network analyzer with an ATN-4112A $S$-parameter test set over the frequency range from 100 MHz to 5 GHz. The electrical lengths due to the SMA connectors at the ports were removed using port extension after a full two-port SOLT calibration. The loss due to the SMA connectors was included in the parameter extraction. The stripline case shown in part C of this section will demonstrate that the loss effects due to the SMA connectors are negligible up to 5 GHz. The dimensions for the four test boards and their highest measurement frequencies are summarized in Table I. The extracted Debye parameters and the frequency limitations for the three Debye test boards are given in Table II.

As seen from Table II, the extracted parameters of the Debye curves for different FR4 dielectric substrates are different. The reason is that the dielectric properties of FR4 depend on many factors, such as manufacturing processes, chemical compositions, shape and orientation of glass fibers, temperature, humidity, etc. These factors might vary significantly, and the parameters of dispersive curves need to be extracted for each board individually.

TABLE II
EXTRACTED DEBYE PARAMETERS FOR THE SUBSTRATES IN THE TEST BOARDS 1, 2, 3 AND THEIR CORRESPONDING FREQUENCY LIMITATIONS

| Board | $f_{TEM\text{-}bound}$ (GHz) | $\varepsilon_s$ | $\varepsilon_\infty$ | $\tau$ (sec) | $\sigma_e$ (S/m) |
|---|---|---|---|---|---|
| #1 | 12 | 4.41 | 4.24 | $3.74\text{x}10^{-11}$ | $3.65\text{x}10^{-3}$ |
| #2 | 4.4 | 4.66 | 4.09 | $1.05\text{x}10^{-11}$ | $6.21\text{x}10^{-3}$ |
| #3 | 3.2 | 4.18 | 3.64 | $1.14\text{x}10^{-11}$ | $6.29\text{x}10^{-3}$ |

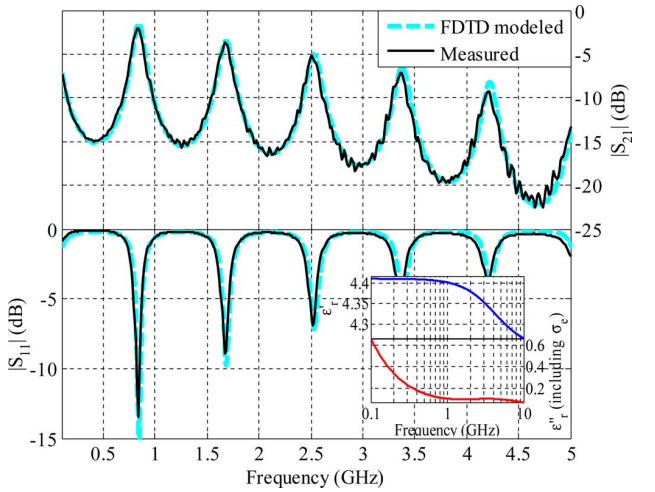


Fig. 6. Measured and modeled $|S_{21}|$ and $|S_{11}|$ for test board 1 and extracted Debye curve.

The extracted FR4 Debye parameters were verified by comparing the measured and the FDTD-modeled $S$-parameters. In the FDTD full-wave modeling, the copper plates of each test board were modeled as a zero thick copper with skin effect. The dielectric spacing between the two copper plates were modeled as a Debye medium with the extracted parameters given in Table II. A recursive convolution procedure was used to implement the Debye dispersion law in the FDTD [28]. The magnitude comparison between the simulation and measurement, and the extracted Debye curves are shown in Fig. 6 for the test board 1. The discrepancy is less than 0.5 dB in $|S_{21}|$, and the difference between resonant frequencies is hard to distinguish. The comparisons shown in Figs. 7 and 8 between the FDTD simulations and measurements also agree well for test board 2 and test board 3, respectively, with the discrepancy of less than 0.7 dB in $|S_{21}|$, and the resonant frequency shift less than 1.67%. The corresponding extracted Debye curves for test boards 2 and 3 are shown in Figs. 7 and 8 as well.

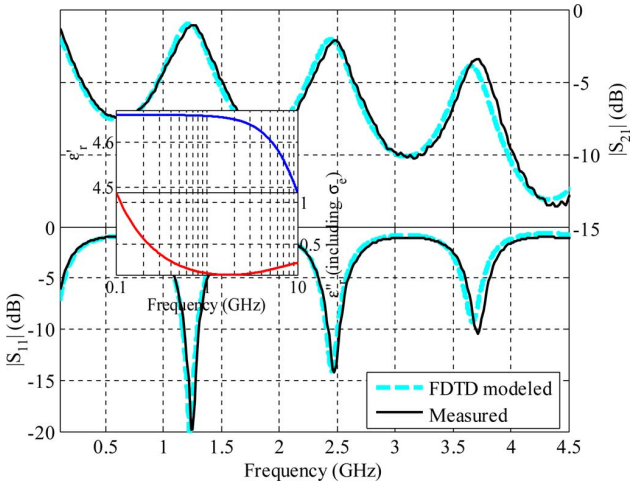


Fig. 7. Measured and modeled $|S_{21}|$ and $|S_{11}|$ for test board 2 and extracted Debye curve.

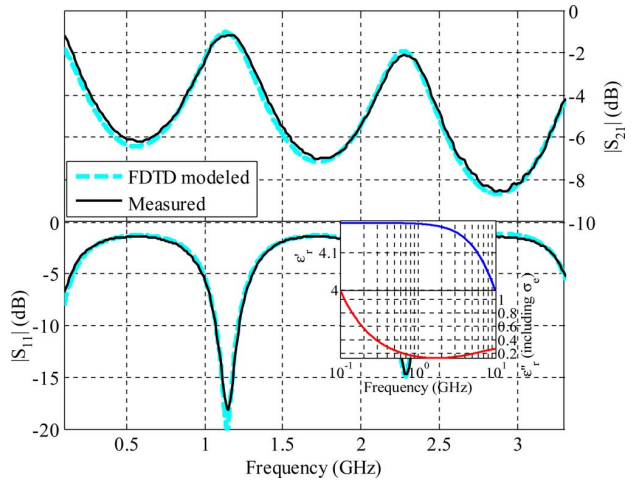


Fig. 8. Measured and modeled $|S_{21}|$ and $|S_{11}|$ for test board 3 and extracted Debye curve.

TABLE III
EXTRACTED LORENTZIAN PARAMETERS FOR A COMPOSITE DIELECTRIC SHEET IN TEST BOARD 4 AND ITS FREQUENCY LIMITATION

| $f_{TEM\text{-}bound}$ (GHz) | $\varepsilon_s$ | $\varepsilon_\infty$ | $\delta$ (rad/s) | $f_0$ (GHz) | $\sigma_e$ (mS/m) |
|---|---|---|---|---|---|
| 10.5 | 2.75 | 2.21 | $9.43\text{x}10^9$ | 1.08 | 5 |

The Lorentzian dielectric parameters were reconstructed from a 0.6-mm-thick composite dielectric sheet with test board 4. The dielectric sheet was composed of a polymer matrix of Teflon-type, filled with a mixture of long aluminum and short carbon fibers [29]. The sheet material is anisotropic. However, its parameters were studied only in the direction normal to the parallel-plate plane. The extracted parameters and the frequency limitation are given in Table III. The material under investigation is a wideband Lorentzian dielectric since the ratio of the resonant line width to the resonant frequency is greater than 1 ($\delta/\omega_0 > 1$) [30]. The effective conductivity loss substantially influences the form of the imaginary part of the composite permittivity. Fig. 9 shows the measured and FDTD-modeled $S$-parameters for the test structure with the Lorentzian

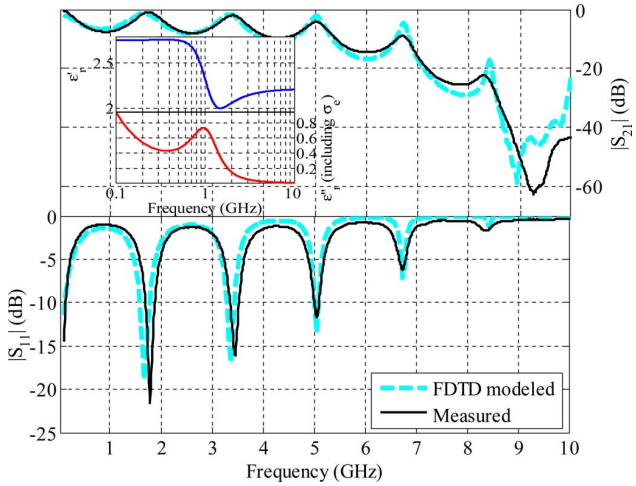


Fig. 9. Measured and modeled $|S_{21}|$ and $|S_{11}|$ for test board 4 and extracted Lorentzian curve.

dielectric and the extracted Lorentzian real and imaginary parts (with an effective conductivity $\sigma_e$). A good agreement is achieved below 9 GHz. At higher frequencies, the discrepancy is due to the anisotropic property of the Lorentzian dielectric substrate, which is not fully studied herein.

### B. Self-Consistency Check and Sensitivity Analysis

The microstrip test board was constructed with the identical material as used for the parallel-plate test board 1 for the purpose of self-consistency examination. The highest measurement frequency and the detailed dimensions of the microstrip test board, referring to Fig. 4, are given in Table IV. Similar to the parallel-plate measurements, the HP 8720ES network analyzer was used, and the port effects due to the electrical length of the SMA connectors were eliminated by port extension. The extracted Debye parameters for the substrate material from the microstrip structure and the test board 1, the relative difference (relative to the extracted value of parallel-plate structure), and the highest frequency limitation for a quasi-TEM/TEM wave propagation on their structures are summarized in Table V.

The agreement in the extraction of $\varepsilon_s$ and $\varepsilon_\infty$ between the parallel plate and the microstrip is less than 1%. However, the difference of $\sigma_e$ is at 6.6%. This is because small variations in $\sigma_e$ and $\tau$ do not significantly impact $|\varepsilon(\omega)|$ for the studied cases, while a small change of $\varepsilon_s$ or $\varepsilon_\infty$ leads to a substantial variation in $|\varepsilon(\omega)|$. These can be seen from the sensitivity analysis of the one-term Debye extraction for the parallel-plate configuration. The sensitivity is defined as [31]

$$S_i = \frac{p_i^0}{\varepsilon_r(\omega)^0}\frac{\partial \varepsilon_r(\omega)}{\partial p_i} \tag{38}$$

where $p_i$ is the $i$th variable and the superscript 0 denotes the reference value shown in Table V for the test board 1. The value $\varepsilon_r(\omega)^0$ is calculated at the reference point over the entire frequency range of interest. The sensitivity of each Debye term

TABLE IV
DIMENSIONS OF THE MICROSTRIP STRUCTURE AND ITS HIGHEST MEASUREMENT FREQUENCY

| Board | $f_{measure\text{-}max}$ (GHz) | w (mm) | d (mm) | z (mm) | a (mm) | t (mm) | b (mm) |
|---|---|---|---|---|---|---|---|
| Microstrip | 5 | 2 | 0.39 | 84 | 4.0 | 0.04 | 16 |

TABLE V
COMPARISON OF EXTRACTED DEBYE PARAMETERS FOR THE SAME SUBSTRATE

| Test board | $f_{TEM\text{-}bound}$ (GHz) | $\varepsilon_s$ | $\varepsilon_\infty$ | $\tau$ (sec) | $\sigma_e$ (S/m) |
|---|---|---|---|---|---|
| Microstrip | 7.8 | 4.44 | 4.27 | $3.67 \times 10^{-11}$ | $3.89 \times 10^{-3}$ |
| Parallel-plate #1 | 12 | 4.41 | 4.24 | $3.74 \times 10^{-11}$ | $3.65 \times 10^{-3}$ |
| Relative discrepancy | N/A | 0.7% | 0.7% | 2.7% | 6.6% |

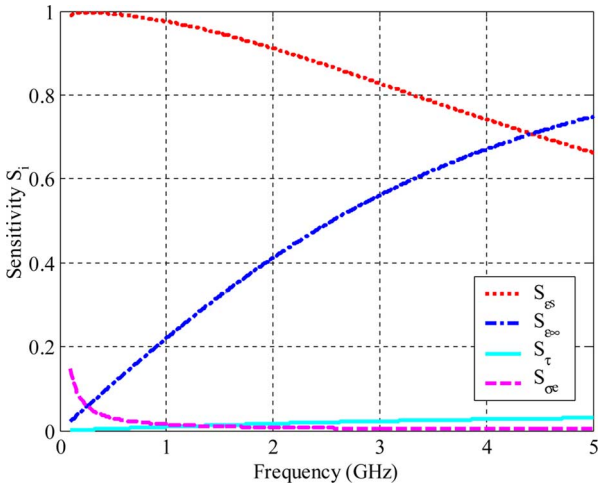


Fig. 10. Sensitivity analysis for one-term Debye parameter extraction.

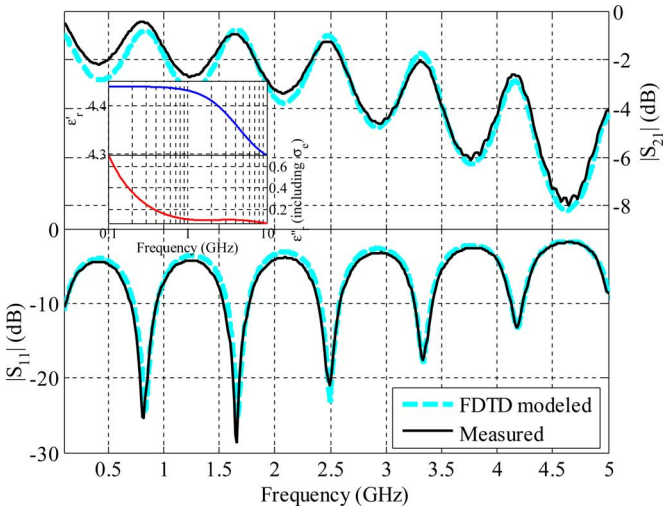


Fig. 11. Measured and modeled $|S_{21}|$ and $|S_{11}|$ for the microstrip line and extracted Debye curve.

can then be estimated as

$$\begin{cases} S_{\varepsilon_s} = \left| \dfrac{4.41}{D^0\,(1+j\omega\tau)} \right| \\ S_{\varepsilon_\infty} = \left| \dfrac{4.24 j\omega\tau}{D^0\,(1+j\omega\tau)} \right| \\ S_\tau = \left| \dfrac{-3.74\times 10^{-11}\,(4.44-4.27)\,j\omega}{D^0\,(1+j\omega\tau)^2} \right| \\ \quad = \left| \dfrac{-6.358\times 10^{-12} j\omega}{D^0\,(1+j\omega\tau)^2} \right| \\ S_{\sigma_e} = \left| \dfrac{-3.65\times 10^{-3} j}{D^0\omega\varepsilon_0} \right| \end{cases} \tag{39}$$

where

$$D^0 = \left(4.24 + \frac{0.17}{1+j3.74\times 10^{-11}\omega} - \frac{j3.65\times 10^{-3}}{\omega\varepsilon_0}\right). \tag{40}$$

The sensitivity of each Debye term relative to the extracted value is shown in Fig. 10 (from 100 MHz to 5 GHz). It demonstrates that the extraction of $\varepsilon_s$ and $\varepsilon_\infty$ is more sensitive than that of $\sigma_e$ and $\tau$. The consequence is that the variation of the extracted $\varepsilon_s$ and $\varepsilon_\infty$ is small, and the variation is large for $\tau$ and $\sigma_e$.

The measured and FDTD-modeled $S$-parameters with Debye parameters from the microstrip extraction and the corresponding Debye curves are shown in Fig. 11. The maximum discrepancy over the entire frequency span is less than 0.6 dB for $|S_{21}|$ and 2 dB for $|S_{11}|$, and the resonant frequency shift is approximately 1.3%. Both real and imaginary parts of pemittivity (involving $\sigma_e$) for the two extracted Debye curves are shown in Fig. 12 with the maximum difference of 0.7% for the real part and 6.1% for the imaginary part, respectively. The comparison between measurements and simulations has demonstrated that the proposed method works well for the extraction of dispersive material parameters for the substrate typically used in PCBs for mixed-signal electronics.

### C. Stripline and Port Effects

One more Debye parameter extraction case was studied for the stripline structure shown in Fig. 5 with an FR4 substrate. Similar to the measurement done for the parallel-plate boards and the microstrip board, a full two-port SOLT calibration with

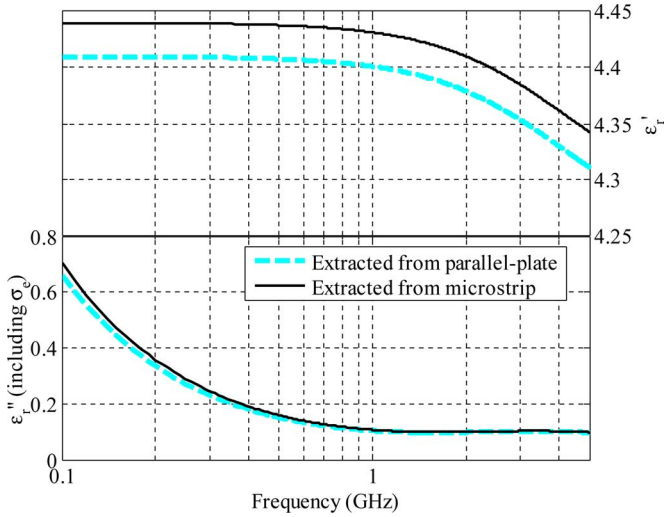


Fig. 12. Real part and imaginary part of the relative permittivity extracted from different structures for an identical material.

TABLE VI
DIMENSIONS OF THE STRIPLINE AND ITS HIGHEST MEASUREMENT FREQUENCY

| Board | $f_{measure\text{-}max}$ (GHz) | w (mm) | d (mm) | z (mm) | b (mm) | t (mm) |
|---|---|---|---|---|---|---|
| Stripline | 5 | 0.32 | 0.36 | 228 | 7.3 | 0.03 |

TABLE VII
EXTRACTED DEBYE PARAMETERS FOR THE STRIPLINE SUBSTRATE AND ITS FREQUENCY LIMITATION

| Test board | $f_{TEM\text{-}bound}$ (GHz) | $\varepsilon_s$ | $\varepsilon_\infty$ | $\tau$ (sec) | $\sigma_e$ (S/m) |
|---|---|---|---|---|---|
| Stripline | 82 | 4.09 | 3.98 | $3.95 \times 10^{-11}$ | $2.58 \times 10^{-3}$ |

port extension was used. The dimensions of the test board and the highest measurement frequency are given in Table VI. The extracted Debye parameters and the frequency limitation for TEM wave propagation are presented in Table VII. The extracted Debye parameters were implemented in full-wave FDTD modeling with copper as zero-thick skin-effect material. The magnitude and phase of $S_{21}$ for the measurement and the simulation are shown in Fig. 13. The difference in magnitude is less than 0.2 dB, and the phase discrepancy is hard to distinguish up to 5 GHz. The Debye curves extracted from the stripline substrate are shown in Fig. 13 as well.

The electrical lengths due to the SMA connectors were removed by port extension from the earlier studied cases. However, the loss due to the SMA connectors was included in the measurements. For the stripline, another measurement was conducted with a TRL calibration to eliminate the port effects [21]. The length of the stripline after TRL calibration was $z' = 202.5$ mm (referring to Fig. 5). The extracted Debye parameters given in Table VII (with port effects) were then used in full-wave FDTD modeling for the piece of pure stripline without port effects. Both in magnitude and phase of $S_{21}$ measurement (TRL calibration) and the FDTD modeling are shown in Fig. 14. The discrepancies shown in Fig. 14 are similar to those shown in Fig. 13 with the maximum difference less than 0.2 dB in magnitude, which indicates that the port effects in the studied cases are not significant, and the proposed material parameter

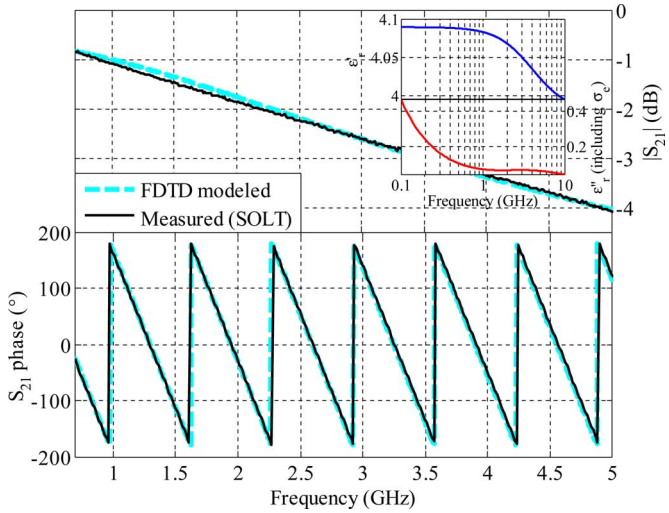


Fig. 13. Measured (SOLT calibration) and modeled $S_{21}$ both in magnitude and phase for the stripline structure.

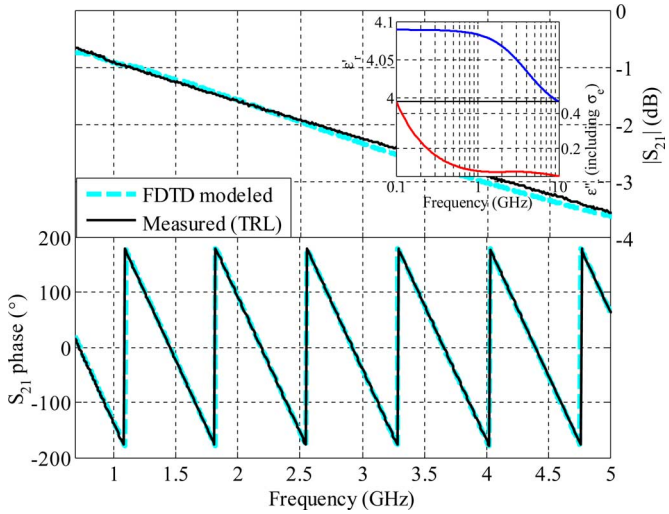


Fig. 14. Measured (TRL calibration) and modeled $S_{21}$ both in magnitude and phase for the stripline structure.

extraction method is valid. The Debye curves used in the full-wave modeling shown in Fig. 14 are exactly the Debye curves shown in Fig. 13.

## V. CONCLUSION

A method for the reconstruction of dispersive dielectric properties (parameters of the Debye and Lorentzian dispersive curves) for PCBs was presented. It was based on the transmission-line theory and application of a GA. Good agreement between the measured and the full-wave FDTD-modeled $S$-parameters was achieved based on the planar transmission-line structures (parallel plate, microstrip, and stripline), when the dielectric parameters of the dispersive substrates were extracted using the proposed method. The self-consistency examination demonstrated that the proposed method was reliable. Port effects in the parameter extraction for the FR-4 substrates were insignificant up to 5 GHz. Using the proposed method with simple planar transmission-line geometries, dielectric properties of

dispersive materials can be extracted effectively under the assumption of TEM/quasi-TEM wave propagation.

## REFERENCES


[1] J. Abdulnour, C. Akyel, and K. Wu, "A generic approach for permittivity measurement of dielectric materials using a discontinuity in a rectangular waveguide or a microstrip line," *IEEE Trans. Microw. Theory Tech.*, vol. 43, no. 5, pp. 1060–1066, May 1995.

[2] J. Huang, K. Wu, and C. Akyel, "Characterization of highly dispersive materials using composite coaxial cells: Electromagnetic analysis and wideband measurement," *IEEE Trans. Microw. Theory Tech.*, vol. 44, no. 5, pp. 770–777, May 1996.

[3] H. Yue and K. L. Virga, "Dielectric constant and loss tangent measurement using a stripline fixture," *IEEE Trans. Compon., Packag., Manuf. Technol. B.*, vol. 21, no. 4, pp. 441–446, Nov. 1998.

[4] D. Han, Y. L. Li, R. A. Vieweg, T. G. Ruttan, and L. A. Polka, "Dielectric material characterization using rough surface transmission lines," in *Proc. Spring 2002 59th ARFTG Conf. Dig.*, Jun., 2002, pp. 49–52.

[5] A. V. Hippel, *Dielectrics and Waves*. New York: Wiley, 1954, pp. 3–86.

[6] M. N. Afsar, J. B. Birch, and R. N. Clarke, "The measurement of the properties of materials," *Proc. IEEE*, vol. 74, no. 1, pp. 183–199, Jan. 1986.

[7] J. Baker-Jarvis, M. Janezic, B. Riddle, C. Holloway, N. Paulter, and J. Blendell, "Dielectric and conductor-loss characterization and measurements on electronic packaging materials," NIST Tech. Note 1520, Nat. Inst. Standards Technol. (NIST), Boulder, CO, Jul. 2001.

[8] J. Baker-Jarvis, M. D. Janezic, B. F. Riddle, R. T. Johnk, P. Kabos, C. L. Holloway, R. G. Geyer, and C. A. Grosvenor, "Measuring the permittivity and permeability of lossy materials: Solid, metals, building materials, and negative-index materials," NIST Tech. Note 1536, Nat. Inst. Standards Technol. (NIST), Boulder, CO, Dec. 2004.

[9] A. Deutsch, T. Winkel, G. V. Kopcsay, C. W. Surovic, B. J. Rubin, G. A. Katopis, B. J. Chamberlin, and R. S. Krabbenhoft, "Extraction of $e_r(f)$ and tan $\delta(f)$ for printed circuit board insulators up to 30 GHz using the short-pulse propagation technique," *IEEE Trans. Adv. Packag.*, vol. 28, no. 1, pp. 4–12, Feb. 2005.

[10] K. S. Kunz and R. J. Luebbers, *The Finite Difference Time Domain Method for Electromagnetics*. Boca Raton, FL: CRC Press, 1993, pp. 123–261.

[11] A. Taflove, *Computational Electrodynamics: The Finite-Difference Time-Domain Method*. Norwood, MA: Artech House, 1995, pp. 227–274.

[12] P. S. Neelakanta, *Handbook of Electromagnetic Materials. Monolithic and Composite Versions and Their Applications*. Boca Raton, FL: CRC Press, 1995, pp. 31–56.

[13] L. D. Landau and E. M. Lifshitz, *Electrodynamics of Continuous Media*. New York: Pergamon, 1960, pp. 256–265.

[14] D. D. Pollock, *Physical Properties of Materials for Engineers*, 2nd ed. Boca Raton, FL: CRC Press, 1993, pp. 499–575.

[15] M. Y. Koledintseva, K. N. Rozanov, G. D. Fazio, and J. L. Drewniak, "Restoration of the Lorentzian and Debye curves of dielectrics and magnetics for FDTD modeling," in *Proc. EMC EUROPE 2002—5th Int. Symp. Electromagnetic Compatibility*, Sorrento, Italy, Sep., pp. 687–692.

[16] L. Davis, *Handbook of Genetic Algorithms*. New York: Van Nostrand Reinhold, 1991, pp. 1–99.

[17] D. Quagliarella, J. Periaux, C. Poloni, and G. Winter, *Genetic Algorithms and Evolution Strategy in Engineering and Computer Science*. New York: Wiley, 1998, pp. 289–309.

[18] Y. Rahmat-Samii and E. Michielssen, *Electromagnetic Optimization by Genetic Algorithms*. New York: Wiley, 1999, pp. 1–93.

[19] B. L. Miller and D. E. Goldberg, "Genetic algorithms, tournament selection, and the effects of noise," Univ. of Illinois at Urbana-Champaign, IlliGAL Rep. 95006, Jul. 1995.

[20] J. Zhang, M. Y. Koledintseva, G. Antonini, K. N. Rozanov, J. L. Drewniak, and A. Orlandi, "Reconstruction of the parameters of Debye and Lorentzian dispersive media using a genetic algorithm," in *Proc. IEEE EMC Symp.*, Boston, MA, Aug. 2003, vol. 2, pp. 898–903.

[21] D. M. Pozar, *Microwave Engineering*, 2nd ed. New York: Wiley, 1998, pp. 56–98.

[22] C. A. Balanis, *Antenna Theory: Analysis and Design*. New York: Wiley, 2001, pp. 736–749.

[23] S. Y. Poh, W. C. Chew, and J. A. Kong, "Approximate formulas for line capacitance and characteristic impedance of microstrip line," *IEEE Trans. Microw. Theory Tech.*, vol. MTT-29, no. 2, pp. 135–142, Feb. 1981.

[24] F. Gardiol and K. Chang, *Microstrip Circuits*. New York: Wiley, 1994, pp. 33–58.

[25] B. C. Wadell, *Transmission Line Design Handbook*. Norwood, MA: Artech House, 1991, pp. 125–137.

[26] H. W. Johnson and M. Graham, *High-Speed Digital Design: A Handbook of Black Magic*. Upper Saddle River, NJ: Prentice-Hall, 1993, pp. 409–439.

[27] R. Mongia, I. Bahl, and P. Bhartia, *RF and Microwave Coupled-Line Circuits*. Norwood, MA: Artech House, 1999, pp. 83–90.

[28] X. Ye, M. Y. Koledintseva, M. Li, and J. L. Drewniak, "FDTD modeling and design of a DC power-bus with dispersive media and surface mount technology components," *IEEE Trans. Electromagn. Compat.*, vol. 43, no. 4, pp. 579–587, Nov. 2001.

[29] A. N. Lagarkov, S. M. Matytsin, K. N. Rozanov, and A. K. Sarychev, "Dielectric properties of fiber-filled composites," *J. Appl. Phys.*, vol. 84, no. 7, pp. 3806–3814, Oct. 1998.

[30] M. Y. Koledintseva, J. L. Drewniak, D. J. Pommerenke, K. N. Rozanov, G. Antonini, and A. Orlandi, "Wideband Lorentzian media in the FDTD algorithm," *IEEE Trans. Electromagn. Compat.*, vol. 47, no. 2, pp. 392–398, May 2005.

[31] A. Saltelli, S. Tarantola, F. Campolongo, and M. Ratto, *Sensitivity Analysis in Practice*. West Sussex, England: Wiley, 2004, pp. 1–56.


**Jianmin Zhang** (S'02–M'07) received the B.S. degree in mechanical engineering from Southeast University, Nanjing, China, in 1985, and the M.S. and Ph.D. degrees in electrical engineering from the University of Missouri-Rolla, Rolla, in 2003 and 2007, respectively.

Since 1985, he has been an Electrical Design Engineer and Electromagnetic Compatibility (EMC) Design Engineer at the Nanjing Electronic Equipment Research Institute, China. In 2007, he joined Cisco Systems, Inc., San Jose, CA, where he is currently a Senior Hardware Engineer. His current research interests include signal integrity, power integrity, SerDes modeling, and electromagnetic interference designs in high-speed digital systems for packages and printed circuit boards.

Dr. Zhang received the Best Symposium Paper Award and the Best Student Symposium Paper Award from the IEEE Electromagnetic Compatibility Society in 2006, and the Conference Best Session Paper Award in signal integrity from the International Microelectronics and Packaging Society in 2007.

**Marina Y. Koledintseva** (M'96–SM'03) received the M.S. degree (with highest honors) and the Ph.D. degree from the Moscow Power Engineering Institute (Technical University) [MPEI (TU)], Moscow, Russia, in 1984 and 1996, respectively.

From 1983 to 1999, she was a Researcher in the Ferrite Laboratory, MPEI (TU), where she was also an Associate Professor from 1997 to 1999. In January 2000, she was a Visiting Professor and joined the Electromagnetic Compatibility (EMC) Laboratory, Missouri University of Science and Technology (MS&T, known as the University of Missouri-Rolla before 2008), where she has been a Research Professor since 2005. Her current research interests include microwave engineering, interaction of electromagnetic fields with ferrites and composite media, their modeling, and application for EMC. She has authored or coauthored about 150 papers and seven patents.

Prof. Koledintseva is a member of the Education, TC-9 Computational Electromagnetics, and TC-11 (Nanotechnology) Committees of the IEEE EMC Society.

**James L. Drewniak** (S'85–M'90–SM'01–F'06) received the B.S., M.S., and Ph.D. degrees from the University of Illinois, Urbana-Champaign, in 1985, 1987, and 1991, respectively, all in electrical engineering.

In 1991, he joined the Electrical and Computer Engineering Department, University of Missouri-Rolla [Missouri University of Science and Technology (MS&T) since 2008], Rolla, where he has been a Full Professor and also one of the Principal Investigators in the Electromagnetic Compatibility (EMC) Laboratory, and where, from 2002 to 2007, he was the Director of the Materials Research Center. His current research interests include EMC in high-speed digital and mixed-signal designs, electronic packaging, microelectromechanical systems, EMC in power-electronic-based systems, and numerical modeling for EMC applications.

**David J. Pommerenke** (M'98–SM'03) was born on April, 11, 1962, in Ann Arbor, MI. He received the Diploma in electrical engineering and the Ph.D degree in transient fields of electrostatic discharge (ESD) from the Technical University of Berlin, Berlin, Germany, in 1989 and 1995, respectively.

During 1989, he was a Research and Teaching Assistant of electromagnetic compatibility (EMC) and high-voltage engineering at the Technical University of Berlin. In 1996, he joined Hewlett Packard. In 2001, he became an Associate Professor in the EMC Group, Missouri University of Science and Technology (MS&T) (formerly known as the University of Missouri-Rolla), Rolla. He is also a member of working group that sets the ESD standards. His current research interests include EMC, ESD, numerical modeling, high-voltage partial discharge detection systems, and design of electronic test and measurement equipment.

**Richard E. DuBroff** (S'74–M'77–SM'84) received the B.S.E.E. degree from Rensselaer Polytechnic Institute, Troy, NY, in 1970, and the M.S. and Ph.D. degrees in electrical engineering from the University of Illinois, Urbana-Champaign, in 1972 and 1976, respectively.

From 1976 to 1978, he was a Postdoctoral Researcher in the Ionosphere Radio Laboratory, University of Illinois, and worked on backscatter inversion of ionospheric electron density profiles. From 1978 to 1984, he was a Research Engineer in the geophysics branch of Phillips Petroleum, Bartlesville, OK. Since 1984, he has been with Missouri University of Science and Technology (formerly University of Missouri-Rolla), Rolla, where he is currently a Professor in the Department of Electrical and Computer Engineering.

**Zhiping Yang** (S'97–M'00–SM'05) received the B.S. and M.S. degrees from Tsinghua University, Beijing, China, in 1994 and 1997, respectively, and the Ph.D. degree from the University of Missouri-Rolla, Rolla, in 2000, all in electrical engineering.

He was a Principal Signal Integrity Engineer at Apple Computer. He was then a Member of the Technical Staff at Nuova Systems, Inc., which was acquired by Cisco Systems, Inc., San Jose, CA, where he is currently the Technical Leader. His current research interests include signal integrity and power integrity methodology development for die/package/board codesign, application of embedded passives, extraction of material properties at high frequency, and high-speed differential signaling technology. He is actively involved with IBIS (I/O Buffer Information Spec) standard activities. His research in power integrity greatly increases IBIS model's simulation accuracy under nonideal power supply conditions. He is a coauthor of the IBIS standard committee BIRD95.6 proposal. He has authored or coauthored more than 20 research papers, and has five issued and three pending U.S. patents.

**Wheling Cheng** received the Bachelor's degree from the Chiao-Tung University, Hsinchu, Taiwan, R.O.C., in 1986, and the Ph.D. degree from Stanford University, Stanford, CA, in 1995.

From 1995 to 1997, she worked for nChip on MultiChip Module development and fabrication. From 1997 to 1999, she worked for logic on signal integrity (LSI) analysis and package design. Since 1999, she has been at Cisco Systems, Inc., San Jose, CA, working on signal integrity and power integrity analysis. Her current research interests include the 3-D modeling of high-speed interconnect and SerDes channel analysis.

**Konstantin N. Rozanov** was born in Moscow, Russia, in 1960. He received the M.S. degree in physics from Moscow State University, Moscow, in 1983, and the Ph.D. degree in electrical engineering from the Institute for High Temperatures, Russian Academy of Sciences, Moscow, in 1991.

Since 1986, he has been with the Scientific Center for Applied Problems in Electrodynamics (SCAPE), Russian Academy of Sciences, Moscow, which was renamed in 1999 as the Institute of Theoretical and Applied Electromagnetics (ITAE), where he has been the Head of the Laboratory for Microwave Composites since 1997. His current research interests include microwave properties of composites and thin magnetic films, design and applications of radar absorbers, and techniques for measurement of microwave material parameters.

**Giulio Antonini** (M'94–SM'05) received the Laurea degree (*summa cum laude*) from the University of L'Aquila, L'Aquila, Italy, in 1994, and the Ph.D. degree from the University of Rome "La Sapienza," Rome, Italy, in 1998, both in electrical engineering.

Since 1998, he has been with the Electromagnetic Compatibility (EMC) Laboratory, Department of Electrical Engineering, University of L'Aquila (UAq), where he is currently an Associate Professor. His current research interests include EMC analysis, numerical modeling, and the field of signal integrity for high-speed digital systems. He has authored or coauthored more than 120 technical papers, three book chapters, and has given nine keynote lectures.

Prof. Antonini received the IEEE TRANSACTIONS ON ELECTROMAGNETIC COMPATIBILITY Best Paper Award in 1997, the IBM Shared University Research Award in 2004, 2005, and 2006, respectively, and the Technical Achievement Award from the IEEE EMC Society "for innovative contributions to computational electromagnetic on the partial element equivalent circuit (PEEC) technique for EMC applications" in 2006. He is the Vice Chairman of the IEEE EMC Italy Chapter, a member of the TC-9 Committee of the IEEE EMC Society, and the Vice Chairman of the TC-10 Committee of the same IEEE Society. He is also a Reviewer for a number of IEEE journals. He has chaired several special sessions at international conferences.

**Antonio Orlandi** (M'90–SM'97–F'07) received the Laurea degree in electrical engineering from the University of Rome "La Sapienza," Rome, Italy, in 1988.

From 1988 to 1990, he was with the Department of Electrical Engineering, University of Rome "La Sapienza." Since 1990, he has been with the Department of Electrical Engineering, University of L'Aquila, L'Aquila, Italy, where he is currently a Full Professor and the Chair of the Electromagnetic Compatibility (EMC) Laboratory. He has authored or coauthored more than 170 technical papers in the field of electromagnetic compatibility in lightning protection systems and power drive systems. His current research interests include the field of numerical methods and modeling techniques to approach signal/power integrity, and EMC/EMI issues in high-speed digital systems.

Prof. Orlandi received the IEEE TRANSACTIONS ON ELECTROMAGNETIC COMPATIBILITY Best Paper Award in 1997, the IEEE EMC Society Technical Achievement Award in 2003, the IBM Shared University Research Award in 2004, 2005, and 2006 and the CST University Award in 2004. He is a member of the Education, TC-9 Computational Electromagnetics and the Chairman of the TC-10 "Signal Integrity" Committees of the IEEE EMC Society, and the Chairman of the TC-5 "Signal Integrity" Technical Committee of the International Zurich Symposium and Technical Exhibition on EMC. From 1996 to 2000, he was an Associate Editor of the IEEE TRANSACTIONS ON ELECTROMAGNETIC COMPATIBILITY, and, from 2001 to 2006, he was an Associate Editor of the IEEE TRANSACTIONS ON MOBILE COMPUTING.